PAPER

Potent "Clicked" MMP2 Inhibitors: Synthesis, Molecular Modeling and Biological Exploration†

Jose María Zapico,[a] Pilar Serra,[a] Josune García-Sanmartín,[b] Kamila Filipiak,[a,c] Rodrigo J. Carbajo,[d] Anne K. Schott,[d] Antonio Pineda-Lucena,[d] Alfredo Martínez,[b] Sonsoles Martín-Santamaría,[a] Beatriz de Pascual-Teresa*[a] and Ana Ramos*[a]

A new series of MMP2 inhibitors is described, following a fragment-based drug design approach. One fragment containing an azide group and a well known hydroxamate Zinc Binding Group in a α-sulfone, α-tetrahydropyrane scaffold, has been synthesized. Water-LOGSY, STD and competition-STD experiments indicate that this fragment binds to the active site of the enzyme. A click chemistry reaction was used to connect the azide to lipophilic alkynes selected to interact selectively with the S1′ subunit of MMP2, as shown by docking and molecular dynamic experiments of the designed compounds. The most potent compounds **18** and **19** displayed an IC_{50} of 1.4 and 0.3 nM against MMP2 respectively, and showed negligible activity towards MMP1 and MMP7, two metalloproteinases which have a shallow S1′ subsite. Compound **18** also showed a promising selectivity profile against some antitarget metalloproteinases, such as MMP8, and considerably less activity against MMP14 (IC_{50} = 65 nM), and MMP9 (IC_{50} = 98 nM), other MMPs characterized by having a deep S1′ pocket and, therefore, more similar to MMP2.

Introduction

Matrix metalloproteinases (MMPs), also called matrixins, are a family of structurally related zinc-containing enzymes that mediate the breakdown of connective tissue and are, therefore, targets for therapeutic inhibitors in many inflammatory, malignant, and degenerative diseases.[1–3]

The vertebrates MMP family includes at least 26 enzymes,[4] among which 23 have been known in humans. They are classified into six groups: Collagenases: MMP1, MMP8, MMP13 and MMP18 (not present in human gene), Gellatinases: MMP2 and MMP9, Stromelysins: MMP3, MMP10 and MMP11, Matrilysin: MMP7 and MMP26, Membrane-type MMPs: MMP14 to MMP17, MMP24 and MMP25 and other MMPs.

Their role in the progression of cancer may involve several mechanisms. Originally, MMPs were thought to mediate invasion and metastasis primarily by matrix remodelling, thereby allowing the tumour cells access to blood and lymphatic vessels. Evidence for this mechanism is based largely on the increased invasiveness of cell lines over-expressing MMPs. More recently, it has been shown that MMPs can play a role in primary tumour growth. This involves the release of stroma-bound growth factors or MMP mediated tumour angiogenesis. Alternatively, remodelling of the extracellular matrix in the vicinity of the primary tumour may provide the special requirements necessary for tumour growth.[5]

Effective MMP inhibitors (MMPIs) are characterized by: 1) a functional group chelating the catalytic zinc ion (zinc-binding group, ZBG); 2) one or more side chains undergoing strong van der Waals interactions with the the enzyme subsites, mainly with S1′; and 3) functional groups providing additional interactions with enzyme backbone.

Zn^{2+}-chelating hydroxamates have been the most frequently used ZBG in MMPI design. However, binding of MMPIs and, most importantly, selectivity have been explained by subtle interactions with key residues belonging to different subsites.[6] This issue has been deeply and accurately addressed by the use of computational techniques, which have pointed to the relevance of S1′ subsite in the regulation of MMP selectivity.[7] Thus, extensive hydrophobic interactions between the lipophilic

[a]Departamento de Química, Facultad de Farmacia, Universidad San Pablo CEU, Urbanización Montepríncipe, 28668, Boadilla del Monte, Madrid, Spain. E-mail: aramgon@ceu.es; bpaster@ceu.es; Fax: (+34)913510496; Tel: (+34)913724796
[b]Center for Biomedical Research of La Rioja (CIBIR) C/Piqueras 98, 26006, Logroño, Spain
[c]Department of Molecular Biology, Faculty of Mathematics and Natural Sciences, The John Paul II Catholic University of Lublin, 20-718, Lublin, Poland
[d]Structural Biology Laboratory, Medicinal Chemistry Department, Centro de Investigación Príncipe Felipe, Avda. Autopista del Saler, 16, 46012, Valencia, Spain

† Electronic supplementary information (ESI) available: IR, ^{1}H and ^{13}C NMR, MS (ESI) and microanalysis data of compounds **14–22**. Evolution of the root-mean-square deviations (RMDS) and some distances monitored for the MD simulations. See DOI: 10.1039/c0ob00852d

This journal is © The Royal Society of Chemistry 2011

Org. Biomol. Chem., 2011, **9**, 4587–4599 | 4587

moieties of the ligand and the S1′ pocket are largely responsible for the binding potencies.[8] Moreover, a novel series of highly selective MMP13 inhibitors (pyrimidine dicarboxamides)[9] with low nanomolar affinities, and a novel series of MMP3 inhibitors (amidinobenzisothiazoles)[10] have been recently reported, which exhibit facile and extensive hydrophobic binding in the S1′ pocket and no interaction with the catalytic Zn^{2+} ion.

After prolonged research, only MMP1, 2, and 7 have been experimentally validated as cancer targets. Inhibition of MMP1 has been hypothesized to be the cause of the clinically observed musculoskeletal syndrome when broad spectrum inhibitors are used.[11,12] On the other hand, reduction of some MMPs such as MMP3, and 8 could enhance tumorgenesis and metastasis, so their inhibition should be avoided.[13,14] MMP9 is a tricky enzyme since its inhibition might be useful in treating patients with early-stage cancers, but MMP9 is an anti-target in patients with advanced disease. So, MMP9 inhibition should also be prevented.[4]

In this work we have focused on the design of selective MMP2 inhibitors. MMP2 plays an important role in cancer, among many other processes, by stimulating tumour growth, angiogenesis and metastasis, through its involvement in the degradation of extracellular matrix. It is overexpressed in human tumour samples and has been identified in association with highly invasive cells. For all these reasons, MMP2 has been considered for many years an important target for the design of anticancer agents. No MMPI has been licensed for the treatment of cancer to date, due mainly to low selectivity, although there are many compounds in clinical development, such as the MMP2 inhibitor incyclinide, a tetracycline derivative which has been tested for cancer metastasis and solid tumours, among other indications, such as allergic conditions, inflammatory, and infectious (fungal) diseases.[15]

Some series of α-sulfone, α-piperidine and α-tetrahydopyran hydroxamates of general structure **1**, including compounds SC-78080/SD-2590 and SC-7774 (Scheme 1) have been described as potent MMP2, MMP9, and MMP13 inhibitors, while sparing MMP1.[12,16–18] For this reason we have used this scaffold in the
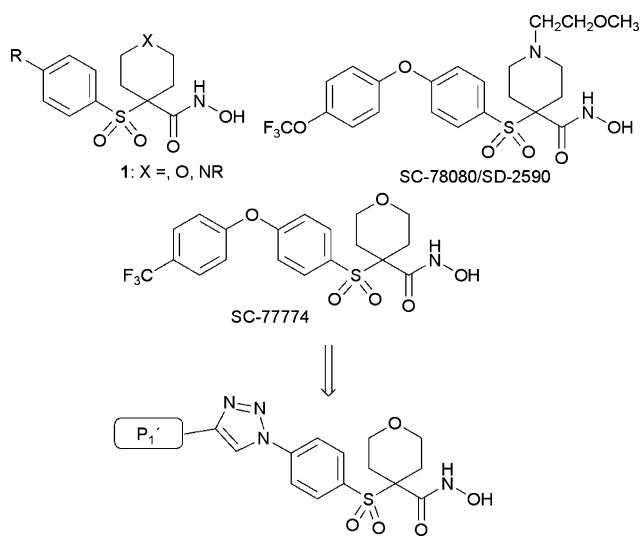
design of new inhibitors, with the aim of increasing the selectivity for MMP2 over MMP9, while maintaining the MMP1-sparing characteristic.

Our approach is based on the use of click chemistry to connect the scaffold containing the hydroxamate ZBG with appropriate subunits designed on the basis of reported selective hydroxamate MMP2 inhibitors (Scheme 1). The Cu(I)-catalyzed azide-alkyne 1,3-dipolar cycloaddition (CuAAC) has been used by several research groups for the discovery of enzyme inhibitors of acetylcholinesterase,[19–21] HIV-1 protease,[22] carbonic anhydrase II,[23] protein tyrosine phosphatases (PTPs),[24] and caspases.[25] It has also been used in an attempt to detect selective MMP inhibitors[26] by the rapid assembly of a library of different succinyl hydroxamates with a series of azides, followed by *in situ* screening for inhibition against MMP7, thermolysin and collagenase. However, they only identified two compounds with activity in the micromolar range for MMP7, inactive for thermolysin and collagenase, but without information about other MMPs.

In this work we present the design and click synthesis of a new potent MMP2 and MMP3 inhibitor (**18**) that is 70-fold more active against MMP-2 than against MMP-9, and completely inactive against MMP1, MMP7 and MMP8. A combination of molecular modelling studies and NMR techniques has been used to reveal the potential interactions that govern the recognition and the binding to MMP2 of the best inhibitors in the synthesized series, and to rationalize the structure-affinity relationships at the molecular level.

Results and Discussion

Chemistry

A series of P1′-diversified MMP2 inhibitors containing the hydroxamate ZBG (Table 1) has been synthesized, using a CuAAC click approach, as shown in Scheme 1. The corresponding azide contains, apart from the ZBG, an α-tetrahydro-2*H*-pyranyl sulfone group (α-THP-sulfone) capable of establishing very relevant hydrogen bond interactions with the enzyme backbone, driving the P1′ group into the S1′ pocket. A series of P1′ groups has been chosen from reported selective MMP2 inhibitors, and have been introduced in the final molecule *via* the corresponding alkyne. Some of the alkynes used are commercially available (Fig. 1), and some had to be synthesized (Scheme 2).
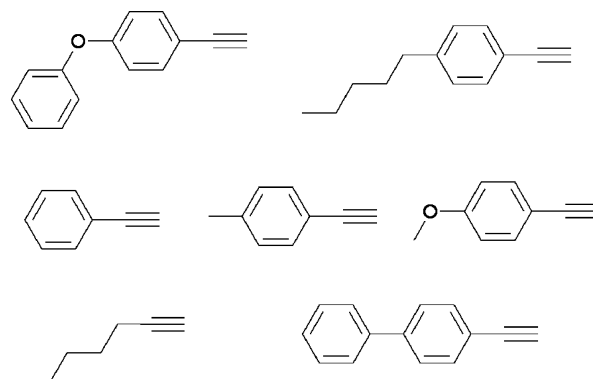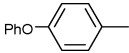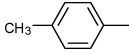

Scheme 1 (From top to bottom.) General structure of MMP2 inhibitors **1** containing a tetrahydropyrane or piperidine heterocycle, structures of SC-78080/SD-2590 and SC-77774, and general structure of the synthesized analogues based on a click synthetic approach.
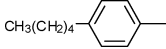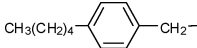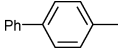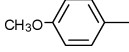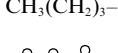
Fig. 1 Commercially available alkynes used in this work.

Table 1 Calculated IC_{50} inhibitory concentrations towards MMP2 and MMP9 for compounds **12–22** and **BiPS**

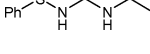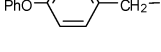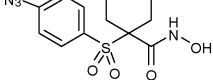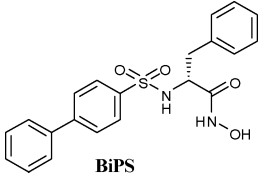| Compound	P1′	Zymogram MMP2 IC_{50}, nM	Zymogram MMP9 IC_{50}, nM	Selectivity MMP9/MMP2
13	PhO–(phenyl)–	10×10^{-3}	32.7×10^{-3}	3.3
14	CH_3–(phenyl)–	2.4×10^{-3}	11.1×10^{-3}	4.5
15	$CH_3(CH_2)_4$–(phenyl)–	7.5×10^{-3}	13.6×10^{-3}	1.8
16	$CH_3(CH_2)_4$–(phenyl)–CH_2–	6.8	—[a]	—
17	(phenyl)–	1.0×10^{-2}	3.1×10^{-2}	3.0
18	Ph–(phenyl)–	1.9×10^{-3}	18.8×10^{-3}	9.7
19	CH_3O–(phenyl)–	9.5×10^{-3}	51.5×10^{-3}	5.4
20	$CH_3(CH_2)_3$–	53×10^{-3}	127.5×10^{-3}	2.4
21	Ph–SO_2–NH–C(O)–NH–ethyl	1.1	>50.00	—
22	PhO–(phenyl)–CH_2–	1.2	>50.00	—
12		0.68	4.4	5.9
BiPS		22.3×10^{-3}	53.4×10^{-3}	2.4

[a] MMP9 data behaved erratically and it was not possible to obtain a specific IC_{50} value. Nevertheless, MMP9 inhibition was lower than the one elicited for MMP2, as shown in Fig. 6A

The detailed synthesis of the ZBG containing azide is shown in Scheme 3. Alkylation of 4-nitrobenzenethiol with methyl 2-bromoacetate gave sulfide **5**, which was oxidized with oxone to give sulfone **6**. The acidic methylene was dialkylated with bis(2-bromoethyl)ether to give sulfone **7**. Saponification of the methyl ester with a H_2O/THF solution of sodium hydroxide and subsequent catalytic hydrogenation of the nitro group in **8** gave amino acid **9**. This was transformed into azide **10** by reaction with *tert*-butyl nitrite and azidotrimethylsilane. Coupling of the carboxylic acid with O-(tetrahydro-2*H*-pyranyl)hydroxylamine

(THP-hydroxylamine) using EDC as amide coupling agent[16] gave the THP-protected hydroxamate **11**, which was subsequently deprotected with a solution of HCl in dioxane to give the desired azide **12**.

For the CuAAC reaction, we used the Cu(II)/ascorbate system, and a variety of conditions were investigated. The use of catalytic amounts of $CuSO_4$ (0,25–2 mol%) in *t*-BuOH/H_2O, and ascorbic acid (5–10 mol%) brought about a very slow transformation of the starting material, without apparent progress of the reaction, even after 3 days. Consequently, the amount of reactants was
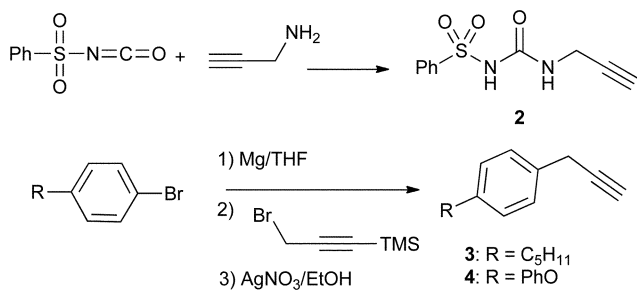
Scheme 2 Synthesis of alkynes 2–4.
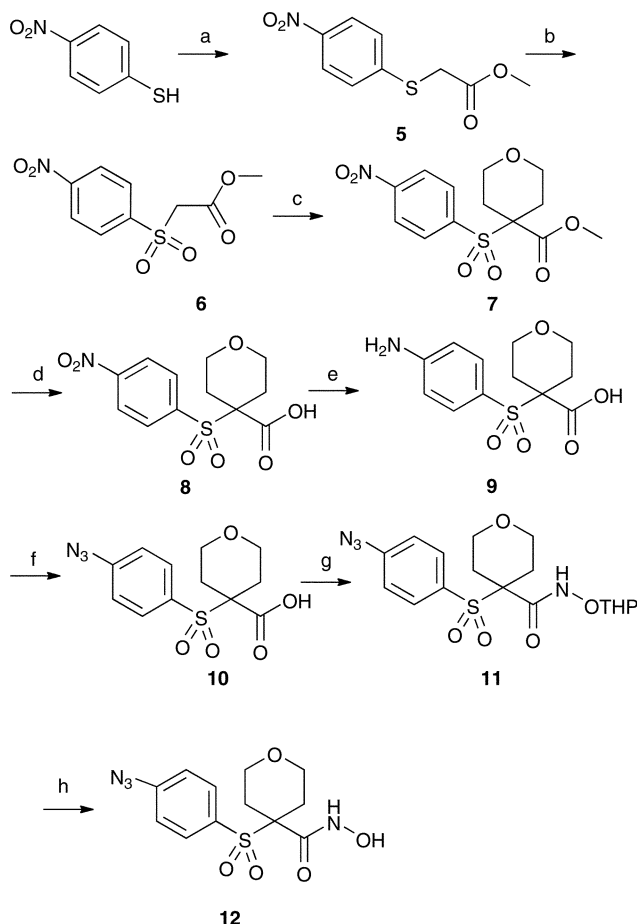
Scheme 3 Synthesis of azide 12. (a) methyl 2-bromoacetate, K₂CO₃, DMF, 98%; (b) oxone, MeOH, H₂O, 90%; (c) O(CH₂CH₂Br)₂, K₂CO₃, DMAP, NBu₄I, DMF, 76%; (d) NaOH, H₂O/THF, 90%; (e) H₂, Pd/C, 95%; (f) t-BuONO, TMSN₃, 94%;(g) NH₂OTHP, EDC, HOBT, DMAP, 94%; (h) HCl, dioxane, 91%.

progressively increased, and the best results were obtained when 0.5 equivalents of CuSO₄ and two equivalents of ascorbic acid were used, leading to compounds 13–22 with moderate yields. Other procedures have been developed where the catalyst is introduced in the form of Cu(0),[27] or CuI.[25] Attempts to carry out the click reaction between azide 12 and phenylacetylene using these methodologies have been unsuccessful, and the starting material was recovered unreacted, even after five days of reaction.

The Cu(I)-catalyzed Huisgen 1,3-dipolar cycloaddition of azides and terminal alkynes is a regioselective process, forming exclusively the 1,4-substituted product. Accordingly, we have obtained

only one isomer in all CuAAC reactions, which in the case of triazole 14 has been characterized as the 1,4-disubstituted isomer by ¹H-NMR (nOe) experiments (see the Experimental Section).

Molecular Modeling

For the designed compounds shown in Table 1, we first evaluated the suitability to act as MMP2 inhibitors by means of docking techniques. There are not many experimental 3D structures of MMP2 available, PDB 1hov being the only complex among MMP2 catalytic domain and an inhibitor, hydroxamate i52 (Fig. 2). Therefore, this structure was considered to perform docking studies. PDB 1hov is an NMR structure composed of 11 models, and the superimposition of all of them showed no relevant changes around the ligand binding region. Previous studies of the binding mode of a set of putative MMP2 inhibitors, including i52, showed no difference in the docking results performed on the 11 models, so we considered only model 1 to carry out the docking studies.[28]
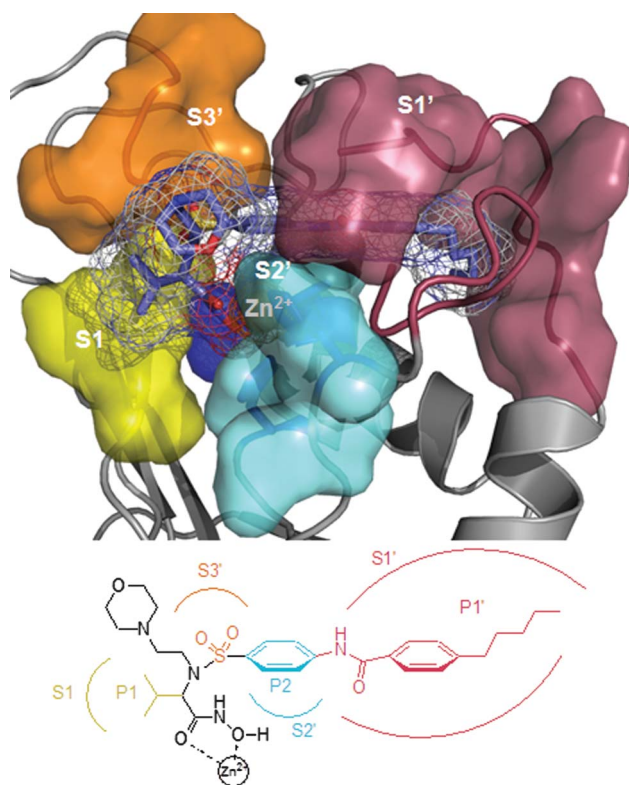
Fig. 2 Chemical structure of compound i52 showing the interactions with the main subsites of MMP2 active site.

Compounds were docked into MMP2 using different approaches (see the Experimental Section), combining rigid and flexible docking procedures and, in some cases, the use of two docking programs, AutoDock and Glide. The predicted binding modes for azide 12, and triazoles 13, 14, 15 (which bears the P1′ group present in compound i52), 18 and 19, were very similar to that of i52, that is, with the two hydroxamate oxygen atoms coordinating the catalytic Zn²⁺ ion, in a divalent fashion, adopting a distorted trigonal bipyramidal geometry, together with the P1′ side chain inside the S1′ binding pocket, and in complete agreement with the experimental data relative to the MMP2-i52

complex. Final end of the P1′ chain occupies a hydrophobic pocket defined by Phe148, Phe115, Leu150 and Thr145, establishing efficient hydrophobic interactions. These interactions are of great relevance for selectivity as Thr145 is an exclusive residue for gelatinases, while Phe148 makes MMP2 distinct from MMP9. The sulfone group perfectly mimics the sulfonamide group from **i52**, establishing hydrogen bonds with the NH groups of Leu83 (S3′) and Ala84 (S1 pocket) (Fig. 3). Ala84 is highly conserved in MMPs and this interaction provides a key anchorage point to the active site.

Fig. 4 Chemical structure of compound **23**.[29]
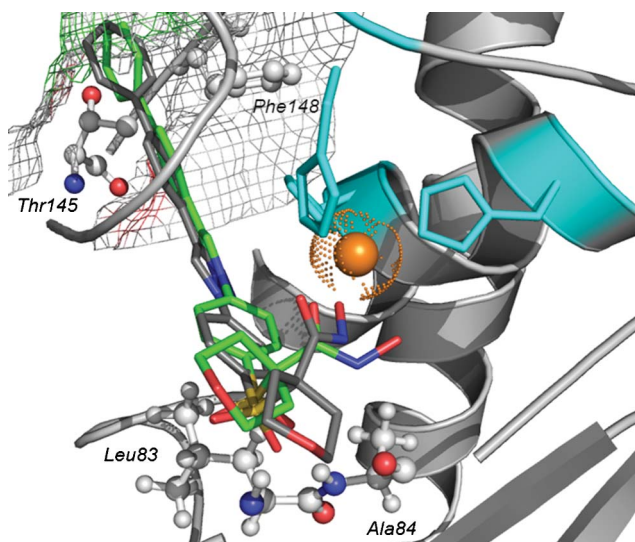
As it will be discussed below, compounds **18** and **19** showed the best profiles of MMP2 inhibition and MMP2 selectivity. Thus, we were prompted to carry out molecular dynamics (MD) simulations of the complexes obtained from the docking studies to validate the proposed binding modes.

Accordingly, MD simulations of both MMP2-**18** and MMP2-**19** complexes (3 ns) were performed. Interactions of metalloproteins with ligands are often difficult to describe effectively due to the limited availability of appropriate force fields. For the treatment of zinc, we have successfully followed the "cationic dummy atom" approach used to impose orientational requirements for zinc ligands, while still allowing flexibility.[30] Globally, all the MMP2-ligand interactions were in agreement with the observations from the docking studies (Fig. 3 and Fig. 5).

Fig. 3 The binding modes of compound **18** in the active site of MMP2 obtained from docking (grey), and MD simulation (green, minimized average structure for the 2 ns–2.5 ns interval of the MD simulation).

Exceptionally, for compound **17**, the predicted binding pose did not show interaction between the hydroxamate group and the catalytic Zn²⁺ ion. The shorter length of the P1′ group allows a deep entrance to the end of the S1′ pocket, so the hydroxamate group establishes a hydrogen bond with NH from Leu83 instead.

For compound **22**, which is one carbon longer than **13**, some docked orientations were predicted, but none of the docking procedures placed the side chain inside the S1′ pocket. Also, compound **16**, which is one carbon longer than **15**, showed predicted binding poses with the P1′ group inside the S1′, but none of them with Zn²⁺ coordination. These results suggest that the introduction of a methylene group between the triazole and the phenyl ring in the P1′ group brings about a loss of activity, most probably related to an increase in flexibility that does not allow proper binding to MMP2.

Compound **21** was designed based on sulfonylurea derivative **23** (Fig. 4), one of the most selective and potent MMP2 hydroxamate inhibitors found in the literature.[29] For this compound AutoDock was not able to find any solution within the binding site and Glide predicted one pose in which the chain is not able to fill the S1′ pocket. The energetically stable conformations of the sulfonylurea group orient the final phenyl ring towards a neighbour pocket defined by the alkyl sp³ carbons of Arg149 and Leu137, but without establishing the efficient hydrophobic interactions that characterize the recognition inside the S1′ pocket.
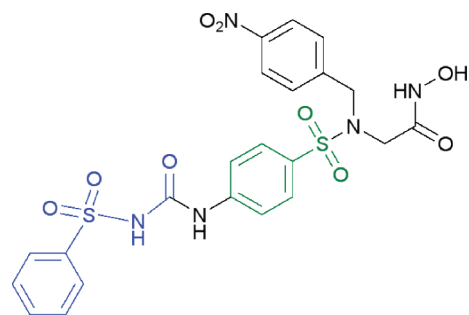

Fig. 5 Minimized average structure for the 2 ns–2.5 ns interval of the MD simulation for the MMP2-**19** complex.

The P1′ chain occupies the S1′ pocket lined with hydrophobic residues Phe148, Phe115, Leu150 and Thr145. Also, it is worth mentioning that the sulfone group establishes stable hydrogen bonds with NH groups from Leu83 and Ala84. In the case of **19**, the P2′ phenyl ring is stacked with His120, while in the case of **18**, the triazol ring is the one which is interacting with His120. These interactions contribute to anchoring the inhibitor within the MMP2 active site and, simultaneously, result in a good bidentated orientation of the hydroxamate group towards the zinc atom. This divalent coordination is maintained along the simulations supporting the proposed binding mode for this novel class of MMP2 ligands (RMSD and monitored distances are available at the ESI†).

This journal is © The Royal Society of Chemistry 2011

Org. Biomol. Chem., 2011, **9**, 4587–4599 | 4591

Biological Evaluation

Zymography. Zimography is a widely used technique to study extracellular matrix-degrading enzymes, such as MMPs, from tissue extracts, cell cultures, serum and urine.[31] It is a simple and very sensitive technique, with a detection limit for MMP2 in gelatin zymography of 10 pg, and able to identify MMPs by the degradation of their substrate. Therefore, zimography allows the detection of highly potent inhibitors, with IC_{50} in the low picomolar range.

Inhibition of MMP2 and MMP9 activities by increasing concentrations of MMPIs was measured by gelatin zymography using human serum as the source of gelatinases. The synthesized compounds were added to the digestion buffer during an overnight incubation, and zymogram bands were analyzed by densitometry. Their inhibitory activity was compared to the one elicited by 2*R*-[(4-biphenylsulfonyl)amino]-*N*-hydroxy-3-phenylpropinamide (**BiPS**), a commercially available MMP2/9 inhibitor (Table 1). Representative zymograms showing the dose-dependent inhibition of MMP2 and MMP9 activities elicited by compounds **16** and **18** are represented in Fig. 6.
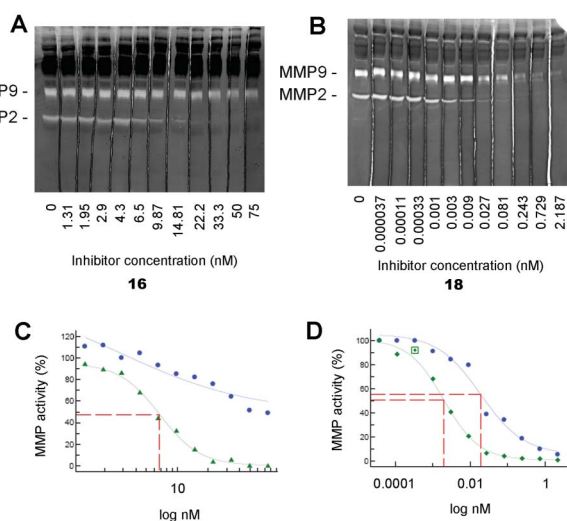

Fig. 6 Representative zymograms showing the dose-dependent inhibition of MMP2 and MMP9 activities elicited by compounds **16** (A) and **18** (B). Bands were quantified by densitometry and graphically represented to obtain the IC_{50} value for each compound and MMP type. For compound **18** (D), the IC_{50} for both MMPs (green diamonds for MMP2, blue dots for MMP9) were calculated, whereas for **16** (C) the values for MMP9 (blue dots) were too erratic and did not allow for a good calculation of the IC_{50} value and only the IC_{50} for MMP2 (green triangles) could be calculated.

Using this methodology all compounds tested showed significant inhibitory activity on MMP2 and MMP9. Our results demonstrate that compounds **13–15**, **17–19** inhibit MMP2 with an IC_{50} in the picomolar range, values which are remarkably higher than those found for **BiPS** in the same experiment (Table 1).[32]

For azide **12**, where the side chain is absent, the inhibition value achieved is three orders of magnitude lower, showing the key role that this group is having in the molecular recognition process. Compounds **16**, **21** and **22** exhibited lower inhibition values than the rest of the triazoles, with IC_{50} in the nanomolar range, and of the same order of magnitude as the value for azide

Table 2 Inhibitory activity of compounds **18** and **19** towards selected MMPs

	Compound **18** IC_{50}, nM[a]	Compound **19** IC_{50}, nM[a]
MMP1	>1000	>1000
MMP2	1.4	0.3
MMP3	17.2	9.6
MMP7	>100	70
MMP8	>100	6.1
MMP9	98	11.3
MMP10	51	7.8
MMP12	3.2	1.2
MMP13	0.9	1.4
MMP14	65	8.2

[a] Concentration required for 50% inhibition of enzyme activity. Standard deviations are less than 10% of mean values in three experiments

12. These results are in agreement with the docking studies that predicted that these compounds are not able to establish efficient hydrophobic interactions inside the S1′ pocket (**21** and **22**) or only in orientations where the hydroxamate group is not coordinating the Zn^{2+} ion (**16**).

Specific MMP2 IC_{50} values of all compounds tested were lower than the corresponding values for MMP9, putting forward a promising MMP2/MMP9 selectivity profile. Taking into account these interesting results, we then proceeded to select the most active and selective compounds (**18** and **19**) in order to submit them for a complete MMP inhibitory profile.

MMPs inhibition profile

Compounds **18** and **19** were selected to carry out studies of selectivity in a panel of ten different MMPs to obtain a complete inhibitory profile. The two compounds were tested in a *MMP Inhibitor Profiling Kit* (Enzo Life Science, Inc), which allows the quantitative measurement of MMP inhibition and was used as described in the Experimental Section.

Table 2 reports MMP inhibitory activities of these compounds as IC_{50} values. Both **18** and **19** show potency as MMP2 and MMP13 inhibitors in the low nanomolar range. Compound **18** showed an IC_{50} = 1.4 nM towards MMP2, and IC_{50} = 0.9 nM towards MMP13, and selectivity over MMP1 and MMP7. The negligible activity of these inhibitors against MMP-1 and MMP-7 is not unexpected. They have been designed to interact with MMP-2, an enzyme characterized by a large adaptable S1′ pocket, while MMP-1 and MMP-7 display short and narrow S1′ pockets.[33,34] Moreover, **18** is also selective *versus* MMP8 and shows a reduced activity against MMP14 (IC_{50} = 65 nM), and MMP9 (IC_{50} = 98 nM), other MMPs characterized by having a deep S1′ pocket and, therefore, more similar to MMP2. The introduction of the rigid biphenyl moiety attached to the triazole subunit, together with the proper length and hydrophobic character of P1′ may be favouring the interaction with the deep hydrophobic S1′ pocket, leading to high inhibitory potency and selectivity for MMP2 and MMP13.

Compound **19**, where the rigid biphenyl has been replaced by the more flexible *p*-methoxyphenyl unit, also exhibits an increased potency with IC_{50} values for MMP2 of 0.3 nM. However, while selectivity *versus* MMP1 is similar to that shown for **18**, the selectivity *versus* the rest of the MMPs is diminished.

NMR studies

NMR is a very powerful biophysical technique to study protein-ligand interactions and, in addition to the analysis of binding events, it can provide relevant structural information. Also, NMR is very sensitive when analysing weak intermolecular interactions. In the current study, two complementary ligand-based NMR techniques covering a wide range of binding affinities, water-LOGSY[35] and STD (Saturation Transfer Difference)[36] have been used. These NMR experiments are designed to evaluate the effect on the ligand upon binding to the protein, which is not required in large amounts nor isotopically labelled. To improve the stability of the recombinantly expressed catalytic domain of MMP2[37] and prevent auto-proteolytic activity, it was necessary to mutate the active site glutamic acid to glutamine, as shown by Rowsell *et al.*[38] This conservative mutation does not affect inhibitor binding in the active site.

All compounds shown in Table 1 were tested for binding to MMP2 by NMR, and competition experiments were recorded using **BiPS**, as a positive control. Fig. 7 shows the water-LOGSY, STD and competition-STD spectra acquired for the azide fragment **12** containing the hydroxamate ZBG. Both water-LOGSY and STD yield unambiguous positive results. The decrease in the intensity of the signals for **12** in the STD experiment acquired in the presence of **BiPS** inhibitor, indicates that both molecules bind to the same site on MMP2.
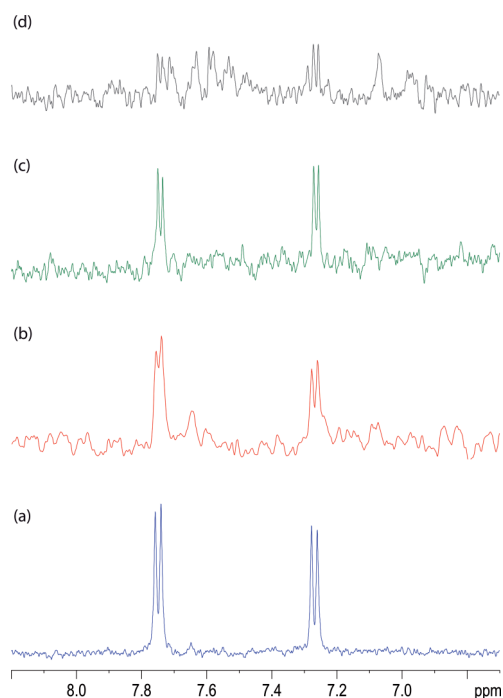

Fig. 7 NMR binding experiments of MMP2 with fragment **12**. (a) Aromatic proton region of the monodimensional ^{1}H NMR of MMP2 (5 μM) and **12** (100 μM). At this protein concentration the signals from MMP2 are not observed. (b) Water-LOGSY and (c) STD experiments show positive signals from the ligand, thus proving the interaction between the protein and **12**. (d) Competition STD experiment after the addition of 200 μM **BiPS**. The reduction of the signals compared to spectrum (c) indicates that both **12** and **BiPS** bind to the same MMP2 site. The extra signals on the spectrum correspond to the **BiPS** molecule.

These experimental results are in complete agreement with our docking predictions, demonstrating the appropriate selection of the azide fragment to carry out fragment-based drug design. Attachment of carefully selected alkynes has led to compounds **13–22** which were also submitted to the same NMR experiments.

Compounds **20** and **21** showed positive results in the interaction with MMP2 and in the competition experiments. Compounds **14**, **17**, **19** and **22** showed positive results in the NMR binding experiments, although their competition assays did not provide conclusive results due to the low solubility of the compounds in water. The rest of the molecules could not be assayed by NMR, not even after the addition of up to 10% DMSO to improve the solubility of the sample.

STD experiments can provide structural information by identifying the epitope of the molecule interacting with the protein, as its signals will see a relatively larger increase in intensity compared to those signals belonging to a region of the molecule not directly involved in the binding interaction. However, from the analysis of the interaction experiments of **12**, **20** and **21**, we could not find a region showing a binding preference over the rest.

Conclusions

A series of α-sulfone, α-tetrahydropyrane hydroxamates was designed based on data from the literature about selective MMP2/MMP9 inhibitors, and exploiting the potential of click chemistry in a fragment based drug design approach. One of the designed fragments contains a hydroxamate ZBG, and its ability to bind the active site of the enzyme was demonstrated by water-LOGSY and STD NMR experiments. A CuAAC reaction was used to connect the ZBG fragment bearing an azide to several carefully selected hydrophobic alkynes. These alkynes were chosen to selectively interact with the hydrophobic S1′ pocket of MMP2. The obtained compounds were evaluated as MMP2 and MMP9 inhibitors in a gelatin zymography using human serum as the source of gelatinases and in a colorimetric assay against a panel of ten MMPs. Among the novel inhibitors, compound **18** presented a promising profile, with low nanomolar activity against MMP2 and MMP13, negligible activity towards MMP1 and MMP7, and a 70-fold higher activity compared to MMP9. It also showed lower activity against MMP10 and MMP14. Docking, molecular dynamics simulations and NMR experiments have been used to analyze the mode of binding and to rationalize the structure-affinity relationships at the molecular level.

The described fragment-based design has proved to be a useful method to detect highly MMP2 active inhibitors, selective over MMP1, with a promising selectivity profile against some antitarget metalloproteinases, such as MMP8, and considerably less activity against MMP9. This approach, together with the information obtained from the computational study, is currently being used in the design of new inhibitors making use of different ZBGs. The lack of water solubility of these compounds could preclude their use in clinics. Current work is directed towards the introduction of basic groups which could improve their pharmacokinetic properties.

Additionally, this approach is especially attractive as it permits the design and efficient synthesis of inhibitors with improved selectivity for one or another MMP by a careful selection of the appropriate alkynes.

Experimental Section

Chemistry

General procedures. Melting points (uncorrected) were determined on a Stuart Scientific SMP3 apparatus. Infrared (IR) spectra were recorded with a Perkin-Elmer 1330 infrared spectrophotometer. ^{1}H and ^{13}C NMR data were recorded on a Bruker 300-AC instrument. Chemical shifts (δ) are expressed in parts per million relative to internal tetramethylsilane; coupling constants (J) are in hertz. Mass spectra were run on a Bruker Esquire 3000 spectrometer. Elemental analyses (C, H, N) were performed on a LECO CHNS-932 apparatus at the Microanalyses Service of the University Complutense of Madrid; unless otherwise stated, all reported values are within $\pm 0.4\%$ of the theoretical compositions. Thin-layer chromatography (TLC) was run on Merck silica gel 60 F-254 plates. Unless stated otherwise, starting materials used were high-grade commercial products.

N-(Prop-2-yn-1-ylcarbamoyl)benzenesulfonamide (2). Benzenesulfonyl isocyanate (5.09 g, 26.38 mmol) was added to a solution of propargylamine (1.48 g, 26.38 mmol) in anhydrous CH_3CN (40 cm^3) under argon. After stirring at room temperature overnight, the reaction mixture was concentrated under vacuum, and the obtained solid was recrystallized from AcOEt to give **2** (5.47 g, 87%) as a white solid, mp 161.8–163.6 °C. ν_{max} (KBr)/cm^{-1} 3354, 3269, 2125, 1705, 1667; δ_H (DMSO-d_6) 3.10 (1H, t, J 2.4, C≡CH), 3.74 (2H, dd, J 2.4 and 5.5, CH$_2$), 6.92 (1H, t, J 5.49, NH-CH$_2$), 7.59–7.71 (3H, m, ArH), 7.89–7.92 (2H, m, ArH), 10.9 (1H, br s, SO$_2$NH); δ_C (DMSO-d_6) 28.9, 73.2, 81.1, 127.3, 129.1, 133.3, 140.2, 151.3. MS (ESI): m/z 260.96 [M+Na]$^+$.

1-Pentyl-4-(prop-2-yn-1-yl)benzene (3). A portion (1 cm^3) of a solution of 1-bromo-4-pentylbenzene (3.00 g, 12.81 mmol) in anhydrous THF (10 cm^3) was added to a mixture of magnesium turnings (0.34 g, 14.04 mmol) and iodine (10 mg) in anhydrous THF (2 cm^3) under argon. When the Grignard reaction began, and after addition of 10 cm^3 of dry THF, the remaining solution of aryl bromide was added dropwise. The reaction mixture was refluxed for 2 h. After cooling to room temperature, the rest of the magnesium was removed by filtration *via* cannula. To the resulting solution was added (3-bromoprop-1-ynyl)trimethylsilane (2.00 g, 10.25 mmol) and the mixture was refluxed for 12 h, cooled and concentrated under vacuum. A solution of 1 N HCl (50 cm^3) was added and the crude was extracted with Et$_2$O. The organic extracts were dried (MgSO$_4$), filtered and evaporated to dryness. The residue was chromatographed on silica gel using hexane as eluent to obtain trimethyl-[3-(4-pentylphenyl)prop-1-ynyl]silane as a colourless oil (708 mg, 21%). ν_{max}/cm^{-1} 2165; δ_H (CDCl$_3$) 0.20 (9H, s, Si(CH$_3$)$_3$), 0.90 (3H, t, J 6.8, CH$_3$), 1.29–1.38 (4H, m, CH_2CH_2CH$_3$), 1.56–1.66 (2H, m, ArCH$_2$CH_2), 2.60 (2H, t, J 7.8, ArCH_2CH$_2$), 3.64 (2H, s, C≡C–CH$_2$), 7.15 (2H, d, J 8.3, ArH), 7.26 (2H, d, J 8.3, ArH); δ_C (CDCl$_3$) 0.1, 14.0, 22.6, 25.7, 31.3, 31.5, 35.5, 86.5, 104.6, 127.7, 128.5, 133.4, 141.1.

A solution of silver nitrate (609 mg, 3,59 mmol) in water (3 cm^3) and EtOH (7 cm^3) was added dropwise to a solution of the TMS-protected alkyne (618 mg, 2.39 mmol) in EtOH (10 cm^3). The solution was stirred at room temperature for 30 min and then, a solution of and KCN (1,58 g, 23,91 mmol) in water (3 cm^3) was

added. The mixture was extracted with Et$_2$O, the organic extracts were washed with water and brine, dried (MgSO$_4$) and evaporated to dryness. The residue was purified by column chromatography on silica gel, using hexane as eluent to afford **3** as a colourless oil (430 mg, 97%) which decomposes on standing. ν_{max}/cm^{-1} 2115; δ_H (CDCl$_3$) 0.92 (3H, t, J 6.4, CH$_3$), 1.29–1.36 (4H, m, CH_2CH_2CH$_3$), 1.56–1.67 (2H, m, ArCH$_2$CH_2), 2.20 (1H, t, J 2.9, C≡CH), 2.61 (2H, t, J 7.3, ArCH_2CH$_2$), 3.60 (2H, d, J 2.9, C≡C–CH$_2$), 7.16 (2H, d, J 7.8, ArH), 7.29 (2H, d, J 7.8, ArH); δ_C (CDCl$_3$) 14.0, 22.5, 24.3, 31.2, 31.4, 35.4, 70.2, 82.1, 127.6, 128.5, 133.1, 141.2.

1-Phenoxy-4-(prop-2-yn-1-yl)benzene (4). The procedure described above was used for the synthesis of **4**. From 1-bromo-4-phenoxybenzene (4,00 g, 16,06 mmol), magnesium turnings (0.42 g, 17.29 mmol), iodine (10 mg) and (3-bromo-1-propynyl)trimethylsilane (2.36 g, 12.35 mmol), and after chromatography using hexane/DCM (95 : 5) as eluent trimethyl-[3-(4-phenoxyphenyl)prop-1-ynyl]silane was produced as a colourless oil (1.15 g, 33%), which decomposes on standing. ν_{max}/cm^{-1} 2160; δ_H (CDCl$_3$) 0.28 (9H, s, Si(CH$_3$)$_3$), 3.71 (2H, s, C≡C–CH$_2$), 7.03–7.09 (4H, m, ArH), 7.13–7.19 (1H, m, ArH), 7.36–7.39 (4H, m, ArH); δ_C (CDCl$_3$) 0.1, 25.4, 86.9, 104.3, 118.6, 119.0, 123.1, 129.1, 129.7, 131.1, 155.8, 157.3.

From trimethyl-[3-(4-phenoxyphenyl)prop-1-ynyl]silane (1,15 g, 4,10 mmol), AgNO$_3$ (1.05 g, 6.15 mmol) and KCN (2,67 g, 41,01 mmol) and after column chromatography using hexane/DCM (9 : 1) as eluent, **4** was produced as a colourless oil (734 mg, 86%) which decomposes on standing. δ_H (CDCl$_3$) 2.22 (1H, t, J 2.9, CH), 3.61 (2H, d, J 2.9, CH$_2$), 6.97–7.04 (4H, m, ArH), 7.08–7.14 (1H, m, ArH), 7.31–7.36 (4H, m, ArH); δ_C (CDCl$_3$) 24.0, 70.5, 81.2, 118.6, 119.1, 123.1, 129.1, 129.7, 130.9, 155.8, 157.3.

Methyl [(4-nitrophenyl)sulfanyl]acetate (5). K$_2$CO$_3$ (5.39 g, 39.02 mmol) was added to a solution of 4-nitrobenzenethiol (5.05 g, 26.01 mmol) in DMF (50 cm^3) at 0 °C. The reaction was stirred for 15 min at 0 °C and methyl bromoacetate (2.65 cm^3, 28.62 mmol) was added. The reaction mixture was stirred overnight at room temperature and then diluted with ethyl acetate (200 cm^3) and washed successively with saturated aqueous NH$_4$Cl and brine. The extract was dried (MgSO$_4$), filtered and evaporated to dryness, and the residue which was chromatographed on silica gel (hexane/AcOEt 85 : 15) to give **5** (5.80 g, 98%) as a white solid, mp 69.8–71.2 °C (EtOH). (Found: C, 47.43; H, 3.93; N, 6.78; S, 14.30. C$_9$H$_9$NO$_4$S requires C, 47.57; H, 3.99; N, 6.16; S, 14.11%); ν_{max} (KBr)/cm^{-1} 1724; δ_H (CDCl$_3$) 3.78 (3H, s, OCH$_3$), 3.80 (2H,s, CH$_2$), 7.43 (2H, d, J = 8.8, ArH), 8.16 (2H, d, J = 8.8, ArH); δ_C (CDCl$_3$) 34.2, 53.0, 124.0, 126.6, 145.3, 145.6, 169.1; MS (ESI): m/z 249.93 [M+Na]$^+$.

Methyl [(4-nitrophenyl)sulfonyl]acetate (6). Oxone® (potassium hydrogen persulfate) (38.69 g 62.93 mmol) was added to a solution of **5** (5.72 g, 25.17 mmol) in MeOH (50 cm^3) and water (5 cm^3) at 0 °C. After stirring at room temperature for 2 h, the crude reaction was filtered and the solid washed with MeOH. The solution was concentrated *in vacuo*, solved in AcOEt, washed with saturated aqueous NaHCO$_3$ and brine. The extract was dried (MgSO$_4$), filtered and evaporated to dryness, to give **6** (5.84 g, 90%) as a yellowish solid, mp 130.3–131.8 °C (AcOEt). (Found: C, 41.74; H, 3.50; N, 5.81; S, 12.47. C$_9$H$_9$NO$_6$S requires C, 41.70;

H, 3.54; N, 5.40; S, 12.37%); ν_{max} (KBr)/cm^{-1} 1740; δ_H (CDCl$_3$) 3.75 (3H, s, OCH$_3$), 4.21 (2H, s, CH$_2$), 8.18 (2H, d, J 8.8, ArH), 8.46 (2H, d, J 8.8, ArH); δ_C (CDCl$_3$) 53.4, 60.4, 124.4, 130.3, 143.9, 151.1, 162.4; MS (ESI): m/z 281.95 [M+Na]$^+$.

Methyl 4-[(4-nitrophenyl)sulfonyl]tetrahydro-2H-pyran-4-carboxylate (7). K$_2$CO$_3$ (4.00 g, 28.93 mmol) was added to a solution of **6** (3.00 g, 11.57 mmol) in DMF (30 cm^3) at 0 °C. The reaction mixture was stirred for 15 min at room temperature and bis-(2-bromoethyl)ether (2.95 g, 12.73 mmol), DMAP (85 mg, 0.69 mmol) and tetra-n-butylammonium iodide (256 mg, 0.69 mmol) were added. Then the mixture was stirred at room temperature 24 h and poured into 1 N HCl (100 cm^3). The solid obtained was filtered, washed with hexane to give **7** as a pale yellow solid (4.66 g, 76%) after recrystallization, mp 192.8–194.6 °C (AcOEt). (Found: C, 47.47; H, 4.56; N, 4.51; S, 9.66. C$_{13}$H$_{15}$NO$_7$S requires C 47.41; H, 4.59; N, 4.25; S, 9.74%); ν_{max} (KBr)/cm^{-1} 3104, 2967, 2867, 1739; δ_H (CDCl$_3$) 2.20–2.34 (4H, m, 2CH$_2$), 3.29 (2H, td, J 12.2, 3.4, 2OCHH), 3.81 (3H, s, CH$_3$), 4.01–4.07 (2H, m, 2OCHH), 8.00 (2H, d, J 8.8, ArH), 8.42 (2H, d, J 8.8 Hz, ArH); δ_C (CDCl$_3$) 28.0, 53.6, 64.6, 72.2, 123.9, 131.7, 140.6, 151.2, 167.2; MS (ESI): m/z 352.06 [M+Na]$^+$.

4-[(4-Nitrophenyl)sulfonyl]tetrahydro-2H-pyran-4-carboxylic acid (8). 1 N NaOH (120 cm^3) was added to a solution of **7** (3.94 g, 11.96 mmol) in THF (40 cm^3) and the mixture was stirred at room temperature for 4 h. The crude reaction was concentrated, suspended in H$_2$O and washed with AcOEt. The aqueous layer was acidified to pH 2 with HCl 3 N and extracted with AcOEt. The organic layer was dried (MgSO$_4$), filtered and evaporated to dryness to give **8** as a white solid (3.40 g, 90%), mp 239.3–240.3 °C (dec). (Found: C, 45.75; H, 4.16; N, 4.72; S, 10.16. C$_{12}$H$_{13}$NO$_7$S requires C, 45.71; H, 4.16; N, 4.44; S, 10.17%); ν_{max} (KBr)/cm^{-1} 3445, 1732; δ_H (DMSO-d_6) 1.96–2.09 (4H, m, 2CH$_2$), 3.14–3.23 (2H, m, CH$_2$O), 3.92–3.97 (2H, m, CH$_2$O), 8.07 (2H, d, J 9.1, ArH), 8.46 (2H, d, J 9.1, ArH); δ_C (DMSO-d_6) 27.9, 64.1, 71.5, 124.3, 132.1, 140.2, 151.1, 167.5; MS (ESI): m/z 338.03 [M+Na]$^+$.

4-[(4-aminophenyl)sulfonyl]tetrahydro-2H-pyran-4-carboxylic acid (9). A solution of **8** (3.94 g, 12.50 mmol) in EtOH (150 cm^3) and H$_2$O (50 cm^3) and 10% Pd/C (250 mg) were introduced into a Parr shaker apparatus, and maintained under a hydrogen pressure of 60 p.s.i for 5 h at room temperature. Palladium was filtered off and the solvent was removed to obtain **9** as a white solid (3.40 g, 95%), mp 227.6–228.8 °C. (Found: C, 50.36; H, 5.25; N, 5.05; S, 11.11. C$_{12}$H$_{15}$NO$_5$S requires C, 50.52; H, 5.30; N, 4.91; S, 11.24%); ν_{max} (KBr)/cm^{-1} 3444, 3363, 3298, 1735; δ_H (DMSO-d_6) 1.82 (2H, td, J 12.8 and 4.9, 2CHH), 2.04 (2H, J 12.8, 2CHH), 3.15 (2H, t, J 11.6, 2OCHH), 3.87 (2H, dd, J 11.6 and 3.7 Hz, 2OCHH), 6.25 (2H, NH$_2$), 6.61 (2H, d, J 8.6, ArH), 8.46 (2H, d, J 8.6, ArH); δ_C (DMSO-d_6) 28.4, 64.3, 70.4, 112.4, 118.7, 131.9, 154.3, 168.1; MS (ESI): m/z 308.06 [M+Na]$^+$.

4-[(4-Azidophenyl)sulfonyl]tetrahydro-2H-pyran-4-carboxylic acid (10). Compound **9** (1.99 g, 6.98 mmol) was dissolved in anhydrous CH$_3$CN (50 cm^3) under argon and cooled to 0 °C in an ice bath. To this solution was added t-BuONO (1.24 cm^3, 10.47 mmol), followed by TMSN$_3$ (1.10 cm^3, 8.38 mmol) dropwise. The reaction mixture was stirred at 0 °C for 30 min, and at room temperature for 3 h. Then, it was evaporated to dryness, and the residue was purified by column chromatography on silica gel

(DCM/MeOH 97.5 : 2.5) to give **10** (2.04 g, 94%) as a yellowish solid, mp 191.4–192.4 °C (dec). (Found: C, 46.47; H, 4.24; N, 13.44; S, 10.28. C$_{12}$H$_{13}$N$_3$O$_5$S requires C, 46.30; H, 4.21; N, 13.50; S, 10.30%); ν_{max} (KBr)/cm^{-1} 3443, 2124, 2099, 1735; δ_H (DMSO-d_6) 1.90–2.07 (4H, m, 2CH$_2$), 3.16 (2H, t, J 12.2 Hz, 2OCHH), 3.93 (2H, dd, J 12.2 and 3.7, 2OCHH), 7.37 (2H, d, J 8.6, ArH), 7.77 (2H, d, J 8.6, ArH); δ_C (DMSO-d_6) 28.0, 64.2, 70.9, 119.7, 130.5, 132.1, 146.1, 167.7; MS (ESI): m/z 333.98 [M+Na]$^+$.

4-[(4-Azidophenyl)sulfonyl]-N-(tetrahydro-2H-pyran-2-yloxy)-tetrahydro-2H-pyran-4-carboxamide (11). HOBT (859 mg, 6.36 mmol), NMM (1.75 cm^3, 15.90 mmol), O-tetrahydro-2H-pyran-2-yl-hydroxylamine (1.24 g, 10.60 mmol) and EDCI (1.42 g, 7.42 mmol) were added to a solution of **10** (1.65 g, 5.30 mmol) in DMF (20 cm^3). The reaction mixture was stirred overnight at room temperature and then diluted with AcOEt (60 cm^3) and washed successively with a saturated aqueous solution of NH$_4$Cl and brine. The organic layer was dried (MgSO$_4$), evaporated to dryness and the solid obtained was recrystallized from EtOH and water to give **11** as an orange solid (1.97 g, 91%), mp 194.2–195.8 °C. (Found: C, 49.83; H, 5.39; N, 13.58; S, 7.82. C$_{17}$H$_{22}$N$_4$O$_6$S requires C, 49.75; H, 5.40; N, 13.65; S, 7.81%); ν_{max} (KBr)/cm^{-1} 3323, 2139, 1693; δ_H (CDCl$_3$) 1.61–1.91 (6H, m, 3CH$_2$), 2.08 (2H, d, CH$_2$) 2.28 (2H, td J 13.2 and 4.9, CH$_2$), 3.46–3.54 (2H, "t", CH$_2$O) 3.70–3.75 (1H, m, 1/2CH$_2$O), 3.97–4.05 (3H, m, 3/2 CH$_2$O), 5.01 (1H, br s, CH), 7.37 (2H, d, J 8.8, ArH), 7.85 (2H, d, J 8.8, ArH), 9.42 (1H, s, NH); δ_C (CDCl$_3$) 18.2, 24.9, 27.7, 28.3, 28.5, 62.3, 64.2, 64.3, 70.0, 101.9, 119.6, 129.6, 132.0, 147.0, 163.9; MS (ESI): m/z 433.12 [M+Na]$^+$.

4-[(4-Azidophenyl)sulfonyl]-N-hydroxytetrahydro-2H-pyran-4-carboxamide (12). To a solution of **11** (1.92 g, 4.69 mmol) in dioxane (10 cm^3) was added 4 N HCl in dioxane (5.86 cm^3, 23.43 mmol) followed by MeOH (10 cm^3). After stirring at room temperature for 2 h, the reaction mixture was concentrated under vacuum and the obtained solid was recrystallized from EtOH and water to give **12** (1.36 g, 89%) as an orange solid, mp 197.2–198.1 °C (dec). (Found: C, 44.37; H, 4.47; N, 16.80; S, 9.70. C$_{12}$H$_{14}$N$_4$O$_5$S requires C, 44.17; H, 4.32; N, 17.17; S, 9.83%); ν_{max} (KBr)/cm^{-1} 3349, 3194, 2142, 1681; δ_H (DMSO-d_6) 1.90 (2H, td, J 12.8 and 4.3, 2CHH), 2.20 (2H, d, J 12.8 H, 2CHH), 3.14 (2H, t, J 11.6, 2OCHH), 3.88 (2H, dd, J 11.6 and 3.7, 2OCHH), 7.35 (2H, d, J 8.6, ArH), 7.77 (2H, d, J 8.6, ArH), 9.23 (1H, s, NH), 11.03 (1H, s, OH); δ_C (DMSO-d_6) 27.4, 63.9, 69.3, 119.6, 130.3, 132.1, 145.9, 160.6; MS (ESI): m/z 349.06 [M+Na]$^+$.

General procedure for the preparation of triazoles. To a suspension, of azide **12** (1 equiv) and the corresponding alkyne (1.2 equiv.) in t-BuOH/H$_2$O (1 : 1,5) was added sodium ascorbate (2 equiv. of freshly prepared 1 M solution in water) and copper(II) sulfate pentahydrate (0.5 equiv. of a 0.25 M solution in water) under argon. The mixture was stirred vigorously overnight, and then diluted with water (20 cm^3) and ice. The precipitate formed was collected by filtration and washed with cold water and hexane. The solid was solved in a DCM : MeOH : NH$_3$ (aqueous) 6 : 3 : 1 mixture, filtered through silica gel and the filtrate was concentrated under vacuum.

N-Hydroxy-4-({[4-(4-phenoxyphenyl)-1H-1,2,3-triazole-1-yl]-phenyl}sulfonyl)tetrahydro-2H-pyran-4-carboxamide (13). From **12** (57.7 mg, 0.18 mmol), 1-ethynyl-4-phenoxybencene (41.2 mg,

This journal is © The Royal Society of Chemistry 2011

Org. Biomol. Chem., 2011, **9**, 4587–4599 | 4595

0.21 mmol), sodium ascorbate (354 μL, 0.35 mmol) and copper(II) sulfate pentahydrate (354 μL, 0.09 mmol) **13** (60 mg, 65%) was produced as a white solid, mp 216.4–217.9 °C (dec). (Found: C, 59.58; H, 4.72; N, 10.35; S, 5.91. $C_{26}H_{24}N_4O_6S$ requires C, 59.99; H, 4.65; N, 10.76; S, 6.16%); v_{max} (KBr)/cm^{-1} 3230, 1669; δ_H (DMSO-d_6) 1.99 (2H, td, J 12.8 and 4.9, 2CHH), 2.26 (2H, d, J 12.8, 2CHH), 3.17 (2H, t, J 11.6, 2OCHH), 3.91 (2H, dd, J 11.6 and 3.7, 2OCHH), 7.08–7.22 (5H, m, ArH), 7.44 (2H, t, ArH), 7.96–8.04 (4H, m, ArH), 8.24 (2H, d, J 8.6, ArH), 9.29 (1H, br s, NH), 9.48 (1H, s, Triazole-H) 11.10 (1H, br s, OH). δ_C (DMSO-d_6) 27.4, 64.0, 69.7, 119.2, 119.3, 119.7, 120.0, 124.0, 125.1, 127.4, 130.3, 132.4, 134.0, 140.6, 147.5, 156.4, 157.2, 160.5; MS (ESI): m/z 521.18 [M+H]$^+$.

N-Hydroxy-4-({4-[4-(4-methylphenyl)-1H-1,2,3-triazole-1-yl]-phenyl}sulfonyl)tetrahydro-2H-pyran-4-carboxamide (14). From **12** (66.3 mg, 0.20 mmol), 1-ethynyl-4-methylbenzene (28.3 mg, 0.24 mmol), sodium ascorbate (406 μL, 0.41 mmol) and copper(II) sulfate pentahydrate (406 μL, 0.10 mmol) **14** (57 mg, 63%) was produced as a yellow solid, m.p. 208.1–209.4 °C (dec).

N-Hydroxy-4-({4-[4-(4-pentylphenyl)-1H-1,2,3-triazole-1-yl]-phenyl}sulfonyl)tetrahydro-2H-pyran-4-carboxamide (15). From **12** (45.3 mg, 0.14 mmol), 1-ethynyl-4-pentylbenzene (28.7 mg, 0.17 mmol), sodium ascorbate (278 μL, 0.28 mmol) and copper(II) sulfate pentahydrate (278 μL, 0.07 mmol) **15** (45 mg, 65%) was produced as a brown solid mp 198.0–199.7 °C (dec).

N-Hydroxy-4-({4-[4-(4-pentylbenzyl)-1H-1,2,3-triazole-1-yl]-phenyl}sulfonyl)tetrahydro-2H-pyran-4-carboxamide (16). From **12** (80 mg, 0.25 mmol), **3** (54.8 mg, 0.29 mmol) sodium ascorbate (490 μL, 0.49 mmol) and copper(II) sulfate pentahydrate (490 μL, 0.12 mmol), **16** (60 mg, 48%) was produced as a white solid, mp 167.8–168.9 °C.

N-Hydroxy-4-{[4-(4-phenyl-1H-1,2,3-triazole-1-yl)phenyl]sul-fonyl}tetrahydro-2H-pyran-4-carboxamide (17). From **12** (71.6 mg, 0.22 mmol), phenylacetylene (26.9 mg, 0.26 mmol), sodium ascorbate (438 μL, 0.44 mmol) and copper(II) sulfate pentahydrate (438 μL, 0.11 mmol), **17** (26.7 mg, 28%) was produced as a white solid mp 228.9–230.5 °C (dec).

N-Hydroxy-4-{[4-(4-biphenyl-4-yl-1H-1,2,3-triazole-1-yl)phen-yl]sulfonyl}tetrahydro-2H-pyran-4-carboxamide (18). From **12** (60 mg, 0.18 mmol), 4-ethynylbiphenyl (39.3 mg, 0.22 mmol) sodium ascorbate (368 μL, 0.37 mmol) and copper(II) sulfate pentahydrate (368 μL, 0.09 mmol) **18** (56 mg, 60%) was produced as a yellow solid, mp 227.7–229.0 °C (dec).

N-hydroxy-4-({4-[4-(4-methoxyphenyl)-1H-1,2,3-triazole-1-yl]-phenyl}sulfonyl)tetrahydro-2H-pyran-4-carboxamide (19). From **12** (100 mg, 0.31 mmol), 4-ethynylanisol (48.6 mg, 0.37 mmol) sodium ascorbate (612 μL, 0.61 mmol) and copper(II) sulfate pentahydrate (612 μL, 0.15 mmol), **19** (86 mg, 61%) was produced as a yellow solid, mp 217.1–218.3 °C (dec).

4-{[4-(4-Butyl-1H-1,2,3-triazole-1-yl)phenyl]sulfonyl}-N-hy-droxytetrahydro-2H-pyran-4-carboxamide (20). From **12** (82.9 mg, 0.25 mmol), 1-hexine (54.8 mg, 0.30 mmol), sodium ascorbate (508 μL, 0.51 mmol) and copper(II) sulfate pentahydrate (508 μL, 0.13 mmol) **20** (67 mg, 65%) was produced as a white solid mp 164.5–166.0 °C (dec).

N-hydroxy-4-[(4-{4-[((phenylsulfonyl)carbamoylamino)methyl]-1H-1,2,3-triazole-1-yl}phenyl)sulfonyl]-tetrahydro-2H-pyran-4-carboxamide (21). From **12** (105.4 mg, 0.32 mmol), **2** (92.3 mg, 0.39 mmol), sodium ascorbate (646 μL, 0.65 mmol) and copper(II) sulfate pentahydrate (646 μL, 0.16 mmol), **21** (98 mg, 79%) was produced as a white solid m.p. 185.0 °C (dec).

N-Hydroxy-4-({[4-(4-phenoxybenzyl)-1H-1,2,3-triazole-1-yl]-phenyl}sulfonyl)tetrahydro-2H-pyran-4-carboxamide (22). From **12** (80 mg, 0.25 mmol), **4** (61.3 mg, 0.29 mmol), sodium ascorbate (490 μL, 0.49 mmol) and copper(II) sulfate pentahydrate (490 μL, 0.12 mmol), **22** (36 mg, 27%) was produced as a white solid mp 138.0–139.3 °C (dec).

Molecular Modelling. Ligand processing

All ligands (together with compound **i52**) were first built using CORINA,[39] in its neutral protonation state and extended conformation. Assignment of the atom types and charge calculations were performed with Sybyl 7.3 (Gasteiger-Marsili charges).[40] A minimization for each compound was first carried out using the program Macromodel.[41] Water was set as solvent, and charges selected from the mol2 file created with Sybyl. The program was set to explore through 500 steps. The force field selected was AMBER. A conformational analysis was then performed to all compounds to be docked by use of the program Macromodel[41] and the Monte Carlo methodology[42] that allows the random variation of the selected torsional angles. The parameters given to Macromodel were set to default with some changes: the force field selected was AMBER, as explained before, and a distance-dependent dielectric constant of 1.0 GB/SA solvation model[43] was selected. The program was set to explore through 500 steps modifying three torsional angles each step. The limit of acceptance was set to 50 kJ mol^{-1} above the instant minimum found. The minimization method selected was conjugated gradient.[44] The convergence RMS to evaluate if two conformers are similar was set to a limit of 2 Å. The criteria of minimization convergence was set to 0.05 (kJ mol^{-1})Å^{-1}, that is, if a minimization step of a structure is not able to improve by more than 0.05 (kJ mol^{-1})Å^{-1} the predecessor structure, the energetic minimum has been achieved.

Superimposition. All the conformers resulting from the conformational search were then superimposed to the ligand **i52** is present in PDB 1hov (model 1). This ligand was previously submitted to the same conformational search analysis and followed the same superimposition procedure in order to validate the methodology. The criteria selected for the superimposition was the maximum number of atoms fitted using the CSR program,[45] and the minimum value of the Root Mean Square Deviation (RMSD). Only the conformers with the higher number of fitted atoms were selected for the docking studies.

Docking Studies with AutoDock3[46]

MMP2 catalytic domain from PDB 1hov (model 1) was employed as macromolecule. For the zinc ion, the parameter set reported by Stote *et al.*[47] was used, which means $r = 1.1$ Å, $\varepsilon = 0.25$ kcal mol^{-1} and a formal charge of +2e. Affinity grid files were generated using the auxiliary program AutoGrid.[48] The grid size was set to $128 \times 60 \times 60$ points with a grid spacing of 0.375 Å containing the S1′, S2′ and S1 subsites, together with

the catalytic zinc. The Lamarckian Genetic Algorithm (LGA) was used as the search engine. The original Lennard-Jonnes and hydrogen-bonding potentials provided by the program were used. Step sizes of 2 Å for translation and 60° for rotation were chosen. A maximum number of energy evaluations was set to 250 000. For each of the 100 independent runs, a maximum number of 27 000 LGA operations were generated on a single population of 100 individuals. Operator weights for crossover, mutation, and elitism were set to 0.80, 0.20 and 1, respectively. The parameters for the docking using LGA were identical for all docking jobs. After docking, the 100 solutions were clustered in groups with Root Mean Square (RMS) deviations less than 1.0 Å. The clusters were ranked by the lowest energy representative of each cluster.

The compounds were studied with no restraints between the ZBG and the zinc atom. Other variables were set to default values using AutoDock Tools (ADT).[46]

We have followed several docking protocols, which include: random docking, in which all possible torsionals of each compound were activated, and the starting point of each conformation was randomly selected by the program; superimposed docking, in which the nitrogen atom from the hydroxamate group was superimposed with the same nitrogen atom of compound **i52**, and selected as starting point of the docking study (in this case all possible torsionals were activated); rigid random docking, in which the starting point of each conformation was randomly selected by the program, but all torsionals were inactivated, so that the docked conformation was the one obtained from the superimposition with ligand **i52**.

Docking Studies with Glide[49–51]

Glide program was used to develop docking studies for all compounds. First, structure of MMP2 catalytic domain obtained from PDB 1hov (model 1) was optimized and minimized using the protein preparation wizard application integrated in the Glide package. Then, interaction maps of the protein binding site were created using the Receptor grid generation application, also included in the Glide package, and selecting ligand **i52** as the centre of the grid box. All compounds were prepared using the Ligprep application. OPLS-2005 force field was selected for both protein and ligands preparation. Docking studies were performed randomly. For each docking study the program was set to explore through 10 000 steps and a maximum number of 10 poses per ligand. The selected docking method was XP (Extra-Precision).[52]

Data analysis. All docking results were manually analyzed. The cut off value for coordinating distances, between the catalytic Zn^{2+} ion and the oxygen atoms (or atom) from the hydroxamic group of the inhibitor, was set to 2.53 Å, as this is the maximum reported distance between a coordinating atom and the MMP zinc ion.[53] For each potential docked solution, angles were measured to confirm they are the optimal ones for the coordination geometries and the conformers were classified into three different categories depending on their coordination geometry with the catalytic zinc ion: a trigonal bipyramidal coordination, a square-based pyramid coordination and no coordinating pattern, using the mean atom distance and angles displacement published by Alberts *et al.* (Fig. 8).[53]

Energies were scrutinized, selecting only those docking solutions with a favourable binding energy ($E_{docked} < 0$ Kcal mol^{-1}).
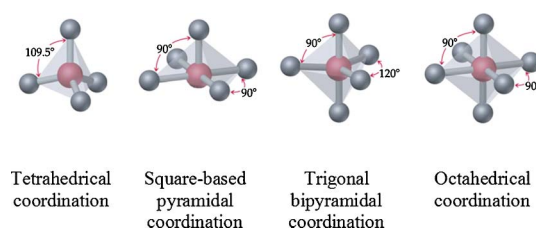

Fig. 8 Different geometries for the coordination of the Zn^{2+} ion found in the citliography for zinc-dependent proteases. MMPIs are found to coordinate by square-based pyramidal or trigonal bipyramidal geometry.[53,54] Zinc ion is represented in red colour and the coordinating atoms are represented in grey (coordinating atoms in MMP are three histidines and one or two atoms of the ligand).

All docking results not matching all these specific characteristics (distances, angles and docked energy) were rejected.

Molecular Dynamics Simulations

Charge calculation. Geometries of **18** and **19** were optimized at the B3LYP/3-21G* level of theory and basis set, followed by a B3LYP/6-31G* single-point energy calculation to determine the electrostatic potential around the molecule, which was subsequently used in the two-stage RESP fitting procedure in order to obtain point charges.[55] All *ab initio* calculations were carried out using Gaussian 03 suite of programs.[56]

Molecular Dynamics Simulations. The following parameters were assigned to zinc atom: van der Waals parameters of $r = 3.1$ Å, and $\varepsilon = 1E^{-6}$ kcal mol^{-1}, charge of zero, and a mass of 50.38 u.m.a. To each of the five dummy atoms covalently bonded to zinc, the following parameters were assigned: charge of +0.4, van der Waals parameters r and ε of zero, and mass of 0.1 u.m.a. Protein-ligand system was first minimized in vacuum for 1000 steps of steepest descent followed by 4000 steps of conjugate gradient using AMBER 9 program.[57] All Cα atoms were restrained to their initial coordinates. Distance and angle restrictions were applied on the catalytic zinc, the dummy atoms and the ZBG atoms. This procedure allowed readjustment of covalent bonds and van der Waals contacts without changing the overall conformation of the protein. The resulting minimized complex was solvated by a box of TIP3P waters which extended at least 8 Å away from any given protein atom (~ 9500 TIP3P water molecules). Periodic boundary conditions were applied and electrostatic interactions were represented using the smooth Particle Mesh Ewald (PME) method[58] with a grid spacing of ~1 Å. First, all hydrogen atoms were minimized for 1000 steps of steepest descent. Next, the position of water molecules was relaxed for 2000 steps of steepest descent followed by 3000 steps of conjugate gradient. Finally, the whole system, including the solute, was energy minimized for 2000 steps of steepest descent plus 3000 steps of conjugate gradients. At this point, the complex was kept frozen and started the thermalization of the solvent by running three 30-ps MD simulations to increase the temperature up to 300 K. Positional constraints were only applied on the ZBG (His120, His124, His130, and the two coordinating oxygen atoms of **18** and **19**) during 500 ps. During the next 500 ps restraints were gradually lowered, followed by 3-ns unrestrained MD simulation (RMSD, Supporting Information†).

This journal is © The Royal Society of Chemistry 2011

Org. Biomol. Chem., 2011, **9**, 4587–4599 | 4597

Zymography

Human blood serum from a healthy volunteer was used as the source of gelatinases.[12] Equal amounts of serum (1.5 µl) were loaded on each well of a 10% gelatin zymogram gel (Invitrogen, Carlsbad, CA, USA). After electrophoresis, the gel was incubated for 30 min in renaturing buffer and then in developing buffer for another 30 min, both at room temperature. At this point, gels were cut into individual strips which were incubated in the presence of the inhibitors in developing buffer overnight at 37° C. Following several washes, the gel fragments were stained with Simply Blue (Invitrogen), destained, and scanned with Odyssey (Li-cor, Lincoln, Nebraska, USA). Gelatinolytic activity for each enzyme (MMP2, 72 kDa; MMP9, 92 kDa) was quantified by image analysis (Image-J, NIH, Bethesda, MD, USA) and the IC_{50} values were calculated with the MS Excel-add-in XLfit (IDBS, UL, Vs. 5.0).

MMPs Inhibition Assays

MMPs activity measurements were performed by using *MMP Inhibitor Profiling Kit* purchased from Enzo Life Science International, Inc., following the manufacturer's protocol with slight modifications. Proteolytic activity was measured using a thiopeptide substrate (Ac-PLG-[2-mercapto-4-methylpentanoyl]-LG—OC_2H_5) where the MMP cleavage site peptide bond has been replaced by a thioester bond.[59,60] Hydrolysis of this bond by MMP produces a sulfhydryl group that reacts with DTNB to form 2-nitro-5-thiobenzoic acid, which was detected by its absorbance at 414 nm (microplate photometer Thermo Scientific Multiscan FC). Enzyme reactions were carried out at 37 °C in a 100 µl final volume of solutions, where the catalytic domains of the corresponding MMP were incubated in triplicate with at least six concentrations of inhibitors. The assay buffer contained the following components: 50 mM HEPES, 10 mM $CaCl_2$, 0.05% Brij-35 and 1mM DTNB at pH 7.5. After addition of substrate, the increase of absorbance was recorded at 1 min time intervals for 20 min. Data were plotted as OD *versus* time for each sample, in order to obtain the reaction velocity (V) in OD min^{-1}. The percentage of residual activity for each compound was calculated using the following formula: % of remaining activity = (V in the presence of inhibitor/Vcontrol) × 100. An inhibitor, NNGH, was included as a prototypic control inhibitor.[61] The concentration of compound that provided 50% inhibition of enzymatic activity (IC_{50}) was determined by semilogarithmic dose-response plots (Graph Pad Prism 5.0).[62]

NMR experiments

All spectra were recorded at 300 K either with a Bruker Ultrashield Plus Avance II 600 MHz or an Avance III 500 MHz spectrometer. The 600 MHz spectrometer is equipped with a 5 mm cryogenically cooled TCI probe, the 500 MHz with a broadband room-temperature TBI probe. A typical NMR sample contained a concentration of 1–5 µM of MMP2 (expression and purification details of this MMP2 construct will be published elsewhere) and 20–100 µM of ligand, in an approximate ratio protein:ligand of 1 : 20, optimal for the water-LOGSY experiments. The sample buffer was 10 mM deuterated-Tris/HCl pH 7.4 with 50 mM NaCl, 0.02% NaN_3, 100 µM $CaCl_2$ and 100 µM $ZnCl_2$. The

concentration of ligand for the Saturation Transfer Difference (STD) experiments kept a ratio protein : ligand 1 : 100. 200 µM of **BiPS** was added for the competition experiments. For each sample, a 1D ^1H reference, a water-LOGSY and a STD experiment were recorded. 8 K points were used for a sweep width of 9,600 Hz and a total of 1 K and 512 scans were accumulated for the water-LOGSY and STD experiments, respectively. In the water-LOGSY experiments, the large bulk water magnetization is partially transferred *via* the protein–ligand complex to the free ligand in a selective manner. A non interacting compound results in negative resonances, whereas protein–ligand interactions are characterized by positive signals or by a reduction in the negative signals obtained in the absence of the protein. In the STD experiment, a positive interaction is recognized by the presence of positive signals, a negative interaction yielding no signals. **BiPS** was purchased from VWR (Barcelona, Spain).

Abbreviations

Abbreviations: DTNB, 5,5′-dithiobis-(2-nitrobenzoic acid); HEPES, 4-(2-hydroxyethyl)-1-piperazineethanesulfonic acid; Brij-35, polyoxyethyleneglycol dodecyl ether; PDB, Protein Data Bank; DCM, dichloromethane; THP, tetrahydropyrane; THF, tetrahydrofurane; EDC, *N*-(3-dimethylaminopropyl)-*N*′-ethylcarbodiimidehydrochloride; TFA, trifluoroacetic acid; DMAP, 4-(dimethylamino)pyridine.

Acknowledgements

References

1 T. E. Cawston, *Pharmacol. Ther.*, 1996, **70**, 163–182.
2 K. M. Bottomley, W. H. Johnson and D. S. Walter, *J. Enzyme Inhib. Med. Chem.*, 1998, **13**, 79–101.
3 I. Massova, L. P. Kotra, R. Fridman and S. Mobashery, *FASEB J.*, 1998, **12**, 1075–1095.
4 C. M. Overall and O. Kleifeld, *Nat. Rev. Cancer*, 2006, **6**, 227–239.
5 J. B. Summers, In *Annual Reports in Medicinal Chemistry*, D. Robertson and J. Plattner, ed. Academic Press, San Diego, 1998, Vol. 33, pp 131–149.
6 I. Bertini, V. Calderone, M. Fragai, A. Giachetti, M. Loconte, C. Luchinat, M. Maletta, C. Nativi and K. J. Yeo, *J. Am. Chem. Soc.*, 2007, **129**, 2466–2475.
7 O. Nicolotti, T. F. Miscioscia, F. Leonetti, G. Muncipinto and A. Carotti, *J. Chem. Inf. Model.*, 2007, **47**, 2439–2448.
8 J. W. Skiles, N. C. Gonnella and A. Y. Jeng, *Curr. Med. Chem.*, 2001, **8**, 425–474.
9 C. K. Engel, B. Pirard, S. Schimanski, R. Kirsch, J. Habermann, O. Klingler, V. Schlotte, K. U. Weithmann and K. U. Wendt, *Chem. Biol.*, 2005, **12**, 181–189.
10 A. Amadasi, P. Cozzini, M. Incerti, E. Duce, E. Fisicaro and P. Vicini, *Bioorg. Med. Chem.*, 2007, **15**, 1420–1429.

4598 | *Org. Biomol. Chem.*, 2011, **9**, 4587–4599

This journal is © The Royal Society of Chemistry 2011

11 T. Tuccinardi, A. Martinelli, E. Nuti, P. Carelli, F. Balzano, G. Uccello-Barretta, G. Murphy and A. Rossello, *Bioorg. Med. Chem.*, 2006, **14**, 4260–4276.

12 D. P. Becker, T. E. Barta, L. J. Bedell, T. L. Boehm, B. R. Bond, J. Carroll, C. P. Carron, G. A. DeCrescenzo, A. M. Easton, J. N. Freskos, C. L. Funckes-Shippy, M. Heron, S. A. Hockerman, C. P. Howard, J. R. Kiefer, M. H. Li, K. J. Mathis, J. J. McDonald, P. P. Mehta, G. H. Munie, Y. Sunyer, C. Swearingen, C. I. Villamil, D. Welsch, J. M. Williams, Y. Yu and J. Yao, *J. Med. Chem.*, 2010, **53**, 6653–6680.

13 M. D. Martin and L. M. Matrisian, *Cancer Metastasis Rev.*, 2007, **26**, 717–724.

14 K. Almholt, A. Juncker-Jensen, O. D. Laerum, K. Dano, M. Johnsen, L. R. Lund and J. Romer, *Mol. Cancer Ther.*, 2008, **7**, 2758–2767.

15 J. Hu, P. E. Van Den Steen, Q. X. Sang and G. Opdenakker, *Nat. Rev. Drug Discovery*, 2007, **6**, 480–498.

16 D. P. Becker, C. I. Villamil, T. E. Barta, L. J. Bedell, T. L. Boehm, G. A. DeCrescenzo, J. N. Freskos, D. P. Getman, S. Hockerman, R. Heintz, S. C. Howard, M. H. Li, J. J. McDonald, C. P. Carron, C. L. Funckes-Shippy, P. P. Mehta, G. E. Munie and C. A. Swearingen, *J. Med. Chem.*, 2005, **48**, 6713–6730.

17 S. A. Kolodziej, S. L. Hockerman, T. L. Boehm, J. N. Carroll, G. A. DeCrescenzo, J. J. McDonald, D. A. Mischke, G. E. Munie, T. R. Fletcher, J. G. Rico, N. W. Stehle, C. Swearingen and D. P. Becker, *Bioorg. Med. Chem. Lett.*, 2010, **20**, 3557–3560.

18 S. A. Kolodziej, S. L. Hockerman, G. A. DeCrescenzo, J. J. McDonald, D. A. Mischke, G. E. Munie, T. R. Fletcher, N. Stehle, C. Swearingen and D. P. Becker, *Bioorg. Med. Chem. Lett.*, 2010, **20**, 3561–3564.

19 R. Manetsch, A. Krasinski, Z. Radic, J. Raushel, P. Taylor, K. B. Sharpless and H. C. Kolb, *J. Am. Chem. Soc.*, 2004, **126**, 12809–12818.

20 W. G. Lewis, L. G. Green, F. Grynszpan, Z. Radic, P. R. Carlier, P. Taylor, M. G. Finn and K. B. Sharpless, *Angew. Chem. Int. Ed. Engl.*, 2002, **41**, 1053–1057.

21 A. Krasinski, Z. Radic, R. Manetsch, J. Raushel, P. Taylor, K. B. Sharpless and H. C. Kolb, *J. Am. Chem. Soc.*, 2005, **127**, 6686–6692.

22 M. Whiting, J. Muldoon, Y. C. Lin, S. M. Silverman, W. Lindstrom, A. J. Olson, H. C. Kolb, M. G. Finn, K. B. Sharpless, J. H. Elder and V. V. Fokin, *Angew. Chem., Int. Ed.*, 2006, **45**, 1435–1439.

23 V. P. Mocharla, B. Colasson, L. V. Lee, S. Roper, K. B. Sharpless, C. H. Wong and H. C. Kolb, *Angew. Chem., Int. Ed.*, 2005, **44**, 116–120.

24 R. Srinivasan, M. Uttamchandani and S. Q. Yao, *Org. Lett.*, 2006, **8**, 713–716.

25 S. L. Ng, P. Y. Yang, K. Y. T. Chen, R. Srinivasan and S. Q. Yao, *Org. Biomol. Chem.*, 2008.

26 J. Wang, M. Uttamchandani, J. Q. Li, M. Y. Hu and S. Q. Yao, *Org. Lett.*, 2006, **8**, 3821–3824.

27 F. Himo, T. Lovell, R. Hilgraf, V. V. Rostovtsev, L. Noodleman, K. B. Sharpless and V. V. Fokin, *J. Am. Chem. Soc.*, 2005, **127**, 210–216.

28 M. A. García, University San Pablo-CEU, Madrid, *PhD Thesis* 2007.

29 A. Scozzafava and C. T. Supuran, *J. Med. Chem.*, 2000, **43**, 1858–1865.

30 Y. P. Pang, *J. Mol. Model.*, 1999, **5**, 196–202.

31 K. Kupai, G. Szucs, S. Cseh, I. Hajdu, C. Csonka, T. Csont and P. Ferdinandy, *J. Pharmacol. Toxicol. Methods*, 2010, **61**, 205–209.

32 Y. Tamura, F. Watanabe, T. Nakatani, K. Yasui, M. Fuji, T. Komurasaki, H. Tsuzuki, R. Maekawa, T. Yoshioka, K. Kawada, K. Sugita and M. Ohtani, *J. Med. Chem.*, 1998, **41**, 640–649.

33 E. Dragoni, V. Calderone, M. Fragai, R. Jaiswal, C. Luchinat and C. Nativi, *Bioconjugate Chem.*, 2009, **20**, 719–727.

34 C. M. Overall and C. Lopez-Otin, *Nat. Rev. Cancer*, 2002, **2**, 657–672.

35 C. Dalvit, P. Pevarello, M. Tatò, M. Veronesi, A. Vulpetti and M. Sundström, *J. Biomol. NMR*, 2000, **18**, 65–68.

36 B. Meyer and T. Peters, *Angew. Chem., Int. Ed.*, 2003, **42**, 864–890.

37 Y. Q. Feng, J. Likos, L. M. Zhu, H. Woodward, J. McDonald, A. Stevens, S. Howard and D. Welsch, *J. Biomol. NMR*, 2000, **17**, 85–86.

38 S. Rowsell, P. Hawtin, C. A. Minshull, H. Jepson, S. M. V. Brockbank, D. G. Barratt, A. M. Slater, W. L. McPheat, D. Waterson, A. M. Henney and R. A. Pauptit, *J. Mol. Biol.*, 2002, **319**, 173–181.

39 J. Gasteiger, C. Rudolph and J. Sadowski, *Tetrahedron Comput. Methodol.*, 1990, **3**, 537–547.

40 J. Gasteiger and M. Marsili, *Tetrahedron Lett.*, 1978, **19**, 3181–3184.

41 F. Mohamadi, N. G. J. Richards, W. C. Guida, R. Liskamp, M. Lipton, C. Caufield, G. Chang, T. Hendrickson and W. C. Still, *J. Comput. Chem.*, 1990, **11**, 440–467.

42 G. Chang, W. C. Guida and W. C. Still, *J. Am. Chem. Soc.*, 1989, **111**, 4379–4386.

43 W. C. Still, A. Tempczyk, R. C. Hawley and T. Hendrickson, *J. Am. Chem. Soc.*, 1990, **112**, 6127–6129.

44 E. Polak and G. Ribiere, *Revue Française d'Informatique et de la Recherche Opérationnelle*, 1969, 16–R1.

45 M. Petitjean, *Comput. Chem.*, 1998, **22**, 463–465.

46 *Autodock 3.0*, The Scripps Institute, 1998.

47 R. H. Stote and M. Karplus, *Proteins: Struct., Funct., Bioinf.*, 1995, **23**, 12–31.

48 *GRID v. 22a*, Molecular Discovery Ltd., 215 Marsh Road, Pinner, Middlesex UK, 2004.

49 *Glide v 2.5021*. Schrödinger, L.L.C., New York, USA, 2003.

50 R. A. Friesner, J. L. Banks, R. B. Murphy, T. A. Halgren, J. J. Klicic, D. T. Mainz, M. P. Repasky, E. H. Knoll, M. Shelley, J. K. Perry, D. E. Shaw, P. Francis and P. S. Shenkin, *J. Med. Chem.*, 2004, **47**, 1739–1749.

51 T. A. Halgren, R. B. Murphy, R. A. Friesner, H. S. Beard, L. L. Frye, W. T. Pollard and J. L. Banks, *J. Med. Chem.*, 2004, **47**, 1750–1759.

52 R. A. Friesner, R. B. Murphy, M. P. Repasky, L. L. Frye, J. R. Greenwood, T. A. Halgren, P. C. Sanschagrin and D. T. Mainz, *J. Med. Chem.*, 2006, **49**, 6177–6196.

53 I. L. Alberts, K. Nadassy and S. J. Wodak, *Protein Sci.*, 1998, **7**, 1700–1716.

54 X. Hu, S. Balaz and W. H. Shelver, *J. Mol. Graphics Modell.*, 2004, **22**, 293–307.

55 C. I. Bayly, P. Cieplak, W. Cornell and P. A. Kollman, *J. Phys. Chem.*, 1993, **97**, 10269–10280 .

56 M. J. Frisch, G. W. Trucks, H. B. Schlegel, G. E. Scuseria, M. A. Robb, J. R. Cheeseman, J. A. Montgomery, Jr., T. Vreven, K. N. Kudin, J. C. Burant, J. M. Millam, S. S. Iyengar, J. Tomasi, V. Barone, B. Mennucci, M. Cossi, G. Scalmani, N. Rega, G. A. Petersson, H. Nakatsuji, M. Hada, M. Ehara, K. Toyota, R. Fukuda, J. Hasegawa, M. Ishida, T. Nakajima, Y. Honda, O. Kitao, H. Nakai, M. Klene, X. Li, J. E. Knox, H. P. Hratchian, J. B. Cross, V. Bakken, C. Adamo, J. Jaramillo, R. Gomperts, R. E. Stratmann, O. Yazyev, A. J. Austin, R. Cammi, C. Pomelli, J. Ochterski, P. Y. Ayala, K. Morokuma, G. A. Voth, P. Salvador, J. J. Dannenberg, V. G. Zakrzewski, S. Dapprich, A. D. Daniels, M. C. Strain, O. Farkas, D. K. Malick, A. D. Rabuck, K. Raghavachari, J. B. Foresman, J. V. Ortiz, Q. Cui, A. G. Baboul, S. Clifford, J. Cioslowski, B. B. Stefanov, G. Liu, A. Liashenko, P. Piskorz, I. Komaromi, R. L. Martin, D. J. Fox, T. Keith, M. A. Al-Laham, C. Y. Peng, A. Nanayakkara, M. Challacombe, P. M. W. Gill, B. G. Johnson, W. Chen, M. W. Wong, C. Gonzalez and J. A. Pople, *GAUSSIAN 03 (Revision C.02)*, Gaussian, Inc., Wallingford, CT, 2004.

57 D. A. Case, T. A. Darden, T. E. Cheatham, III, C. L. Simmerling, J. Wang, R. E. Duke, R. E. Luo, K. M. Merz, D. A. Pearlman, M. Crowley, R. C. Walker, W. Zhang, B. Wang, S. Hayik, A. Roitberg, G. Seabra, K. F. Wong, F. Paesani, X. Wu, S. Brozell, V. Tsui, H. Gohlke, C. Yang, J. Tan, J. Mongan, V. Hornak, G. Cui, P. Beroza, D. H. Mathews, C. Schafmeister, W. S. Ross, P. A. Kollman *AMBER 9*, University of California, San Francisco, 2006.

58 T. A. Darden, D. York and L. G. Pedersen, *J. Chem. Phys.*, 1993, **98**, 10089–10092.

59 H. Weingarten and J. Feder, *Anal. Biochem.*, 1985, **147**, 437–440.

60 H. Weingarten, R. Martin and J. Feder, *Biochemistry-Moscow*, 1985, **24**, 6730–6734.

61 L. J. MacPherson, E. K. Bayburt, M. P. Capparelli, B. J. Carroll, R. Goldstein, M. R. Justice, L. Zhu, S. Hu, R. A. Melton, L. Fryer, R. L. Goldberg, J. R. Doughty, S. Spirito, V. Blancuzzi, D. Wilson, E. M. O'Byrne, V. Ganu and D. T. Parker, *J. Med. Chem.*, 1997, **40**, 2525–2532.

62 *Graph Pad Prism version 5.0 for Windows*, Graph Pad Software Inc., San Diego, California, USA, 2007.

This journal is © The Royal Society of Chemistry 2011

Org. Biomol. Chem., 2011, **9**, 4587–4599 | 4599